REC8-cohesin, chromatin and transcription orchestrate meiotic recombination in the Arabidopsis genome

3

Christophe Lambing¹, Andrew J. Tock¹, Kyuha Choi¹, Stephanie D. Topp¹, Pallas C.
Kuo¹, Alexander R. Blackwell¹, Xiaohui Zhao¹, Kim Osman², James D. Higgins³, F.
Chris H. Franklin² and Ian R. Henderson^{1*}

7

¹ Department of Plant Sciences, University of Cambridge, Cambridge, CB2 3EA, United
 9 Kingdom

10 ² School of Biosciences, University of Birmingham, Birmingham, B15 2TT, United 11 Kingdom

³ Department of Genetics and Genome Biology, University of Leicester, Leicester, LE1
 7RH, United Kingdom

14

15 *Correspondence: irh25@cam.ac.uk
16

17 Abstract:

18 19 During meiosis chromosomes undergo DNA double-strand breaks (DSBs) that can be 20 repaired using a homolog to produce crossovers, which creates genetic diversity. 21 Meiotic recombination occurs coincident with homolog pairing and polymerization of 22 the meiotic axis and synaptonemal complex (SC). REC8-cohesin is required to connect 23 chromosomes to the axis and to organize axis polymerization. However, control of 24 REC8 loading along chromosomes, in relation to chromatin, transcription and 25 recombination, is not yet fully understood. Therefore, we performed REC8 ChIP-seq in 26 Arabidopsis, which revealed strong enrichment in centromeric heterochromatin. REC8 27 abundance correlates with suppression of meiotic DSBs and crossovers, despite axis 28 loading of SPO11-1 in these regions. Loss of the heterochromatic marks H3K9me2 29 and non-CG DNA methylation in kyp/suvh4 suvh5 suvh6 mutants causes remodeling of 30 REC8 and gain of meiotic recombination locally in repeated sequences, although 31 centromere cohesion is maintained. In the chromosome arms, REC8 is enriched within 32 gene bodies, exons and GC-rich sequences, and anti-correlates with transcription. 33 Highest REC8 occupancy occurred in facultatively silent, H3K27me3-modified genes. 34 Using immunocytology we show that axis polycomplexes form in rec8 mutants that 35 recruit recombination foci with altered stoichiometry, leading to catastrophic nonhomologous recombination. Therefore, REC8 plays a key role organizing meiotic 36 37 chromosome architecture and promoting high-fidelity interhomolog recombination. 38 Despite this pro-recombination role, local REC8 enrichment associates with DSB 39 repression at the fine scale, which is consistent with the tethered-loop/axis model. 40 Coincident with its organizational role during meiosis, REC8-cohesin occupancy along 41 the chromosomes is shaped by multiple chromatin states and transcription.

Cohesin, REC8, meiosis, recombination, crossover, H3K9me2, DNA methylation.

42

43 Keywords:

44

45 46

47

- 48
- 49
- 50
- 51
- 52

53 Introduction:

54

55 Cohesin complexes form ~35–50 nm rings that can topologically embrace one or more 56 DNA helices (Uhlmann 2016; Nasmyth and Haering 2009; Peters et al. 2008). Cohesin 57 rings consist of paired structural maintenance of chromosomes (SMC) proteins that 58 interact at hinge and ATPase head domains, with the head regions clamped by an α -59 kleisin (Gligoris and Löwe 2016). DNA can enter and exit cohesin rings at the subunit 60 interfaces, and the rings undergo dynamic cycles of association and disassociation 61 with chromosomes (Uhlmann 2016; Nasmyth and Haering 2009; Peters et al. 2008). 62 Cohesin complexes regulate diverse nuclear processes, including chromosome 63 condensation, segregation, gene expression and DNA replication, recombination and 64 repair (Uhlmann 2016; Nasmyth and Haering 2009; Peters et al. 2008). Cohesin 65 complexes containing the α -kleisin REC8 also play critical roles in controlling meiotic 66 chromosome segregation and interhomolog recombination.

67

68 During meiosis eukaryotic genomes undergo DNA double-strand breaks (DSBs) 69 generated by SPO11 topoisomerase-like complexes (Keeney et al. 1997; Baudat et al. 70 2013). Meiotic DSBs can enter an interhomolog repair pathway to produce reciprocal 71 crossovers, which creates genetic diversity (Hunter 2015). Following meiotic S-phase, 72 sister chromatids form co-aligned chromatin loops connected to axial element polymers 73 via REC8-cohesin complexes (Zickler and Kleckner 1999). The meiotic axis includes 74 HORMA domain proteins (e.g. ASY1) (Armstrong et al. 2002), and interacting partners 75 (e.g. ASY3) (Ferdous et al. 2012), which promote interhomolog recombination. 76 Although REC8-cohesin plays essential roles in establishing the tethered-loop/axis 77 architecture, its role in regulation of meiotic recombination is complex. For example, 78 budding yeast cohesin and axis components are required to additively promote meiotic 79 DSB repair (Klein et al. 1999; Kim et al. 2010), whereas local Rec8 enrichment 80 suppresses DSB formation in both budding and fission yeast (Panizza et al. 2011; 81 Storlazzi et al. 2008; Nambiar and Smith 2018). As meiosis proceeds, HORMA 82 proteins become depleted, as synaptonemal complex (SC) components are installed 83 (e.g. ZYP1), until synapsis completes at pachytene (Ferdous et al. 2012; Lambing et al. 84 2015; Higgins et al. 2005). Hence, REC8-cohesin, axis and SC proteins play tightly 85 integrated roles in establishing a chromosome structure that favors interhomolog repair 86 during meiosis.

87

88 SPO11 and its accessory factors dynamically associate with the axis in fungi and 89 mammals during DSB formation, and DNA repair occurs at axis-associated sites 90 (Stanzione et al. 2016; Blat et al. 2002; Panizza et al. 2011; Baudat et al. 2013; 91 Nambiar and Smith 2018; Pan et al. 2011; Sommermeyer et al. 2013; Acquaviva et al. 92 2013). Budding yeast DSB hotspots occur within nucleosome-free regions in the 93 chromatin loops, in proximity to H3K4me3-modified nucleosomes at gene 5'-ends (Pan 94 et al. 2011; Borde et al. 2009). Direct interactions occur between the Spp1 complex, 95 which catalyzes and binds to H3K4me3, and the meiotic axis protein Mer2 96 (Sommermeyer et al. 2013; Acquaviva et al. 2013). This supports a model where loop 97 DNA sequences are tethered to the axis via specific chromatin modifications during 98 DSB formation and repair. Interactions occur between functionally related components 99 in mammals, including H3K4me3, CXXC1, IHO1 and PRDM9 (Parvanov et al. 2017; 100 Imai et al. 2017), and plant crossovers are positively correlated with gene density and 101 H3K4me3 (Choi et al. 2013). Therefore, euchromatic marks likely play conserved roles 102 in recruiting loop DNA to the axis during meiotic recombination. Transcription itself 103 plays an important role in shaping cohesin accumulation in gene-rich regions in mitosis 104 and meiosis, and can therefore also influence recombination (Lengronne et al. 2004; 105 Bausch et al. 2007; Sun et al. 2015; Busslinger et al. 2017).

106 In contrast to euchromatin, meiotic recombination is typically suppressed in 107 heterochromatin (Underwood et al. 2018; Choi et al. 2018; Ellermeier et al. 2010). 108 Heterochromatin is repeat and transposon-dense, late-replicating, suppressed for RNA 109 polymerase II transcription and densely modified with epigenetic marks including DNA 110 and H3K9 methylation (Janssen et al. 2018). Heterochromatic marks including DNA 111 and H3K9 methylation are sufficient to silence meiotic recombination hotspot activity in 112 plants, fungi and mammals (Zamudio et al. 2015; Yelina et al. 2015; Maloisel and 113 Rossignol 1998). Cohesin is also strongly enriched in the centromeres and 114 pericentromeric heterochromatin of animals and fungi (Tanaka et al. 1999; Mizuguchi 115 et al. 2014; Sun et al. 2015; Blat et al. 2002; Klein et al. 1999; Bernard et al. 2001; 116 Watanabe and Nurse 1999). In fission yeast, centromeric cohesin enrichment requires 117 heterochromatin protein Swi6 and H3K9 methylation (Bernard et al. 2001; Nonaka et al. 118 2002; Mizuguchi et al. 2014), implying a direct connection between heterochromatic 119 epigenetic marks and cohesin recruitment. However, mouse centromeric cohesion is 120 maintained during mitosis in suv39h-1 suv39h-2 H3K9 methylation mutants, although 121 local cohesin remodeling occurs on specific repeats (Koch et al. 2008; Guenatri et al. 122 2004). Therefore, the functional relationships between cohesin, chromatin state and 123 transcription during meiosis, and the consequences for interhomolog recombination, 124 remain incompletely understood.

125

126 Here we use a comprehensive array of genetic, genomic and immunocytological 127 approaches to investigate the role of Arabidopsis REC8 in orchestrating meiotic 128 chromosome architecture and recombination, and its functional interactions with 129 chromatin and transcription. We show that rec8 mutants undergo defective axis polycomplex formation, which associates with catastrophic non-homologous 130 131 recombination. Using REC8 ChIP-seg we show strong enrichment in centromeric heterochromatin and within specific classes of RNA transposable elements. REC8 132 133 levels anti-correlate with meiotic DSBs (SPO11-1-oligos) and crossovers at both the 134 chromosome and fine scales. To directly test the role of heterochromatin on cohesin 135 loading, we performed REC8 ChIP-seq in kryptonite (kyp/suvh4) suvh5 suvh6 triple 136 mutants, which lose H3K9me2 and non-CG DNA methylation. We observed 137 remodelling of cohesin and DSB landscapes in repeated sequences in kyp suvh5 138 suvh6, although centromere cohesion is maintained, meaning that Arabidopsis more 139 closely resembles mice than fission yeast. Transcriptional changes in kyp suvh5 suvh6 140 are associated with remodeling of REC8 occupancy and meiotic DSBs in both genes 141 and transposable elements at the fine-scale. At the cytological scale, we show that 142 rec8 axis polycomplexes are able to recruit the recombination machinery, although with 143 altered stoichiometry. The rec8 polycomplexes undergo synapsis and ultimately cause 144 non-homologous recombination. Hence, REC8-cohesin organizes meiotic chromosome 145 architecture and high-fidelity homologous recombination, and is simultaneously 146 influenced by both chromatin state and transcription.

147 148

149

150

- 151 152
- 153
- 154
- 155
- 156
- 157
- 158

159 **Results**:

160

161 162

1 Complementation of *rec8* meiotic catastrophe via epitope tagging

163 To detect REC8 during meiosis we inserted 3×HA or 5×Myc epitopes into a genomic 164 clone and transformed rec8-3/+ heterozygotes. In wild type meiosis, chromatin matures 165 from thin threads at leptotene, to thick paired axes at pachytene with condensed 166 heterochromatin, until five bivalents connected via chiasmata are evident at metaphase 167 I (Fig. 1A and Supplemental Fig. S1A). In contrast, no axis differentiation occurs in rec8 168 chromatin, which is present as a diffuse mass during mid-prophase I although the 169 proportion constituting heterochromatin is not significantly different (Mann-Whitney-170 Wilcoxon (MWW) test, P=0.55) (Fig. 1A, Supplemental Fig. S1A-S1B and 171 Supplemental Table S1). The entangled chromatin mass in *rec8* proceeds to fragment 172 at metaphase I, causing complete sterility (Fig. 1A) (Cai et al. 2003; Chelysheva et al. 173 2005). We observed that epitope-tagged REC8 constructs complemented rec8 meiotic 174 phenotypes, including (i) axis formation during prophase I, (ii) the presence of five 175 bivalents at metaphase I and (iii) chiasmata counts (Fig. 1A, Supplemental Fig. S2A 176 and Supplemental Table S2).

177

178 To analyze REC8 accumulation on chromosomes we immunostained male meiocytes 179 and observed co-localization with chromatin from leptotene onwards, including within 180 heterochromatin (Fig. 1B and Supplemental Fig. S2B–S2C). REC8 and chromatin co-181 localize as pairing and synapsis occurs, with strong co-staining at pachytene (Fig. 1B 182 and Supplemental Fig. S2B-S2C). REC8 persists on bivalents through diakinesis and 183 metaphase I (Fig. 1B and Supplemental Fig. S2B), as reported (Chelysheva et al. 184 2005; Cai et al. 2003). No signal was detected in non-transgenic wild type meiocytes, 185 or somatic cells of the epitope-tagged lines (Fig. 1B and Supplemental Fig. S2B). We 186 also performed western blotting on meiotic-stage flowers, which revealed bands of the 187 expected size, in addition to bands with a ~20 kDa higher molecular mass 188 (Supplemental Fig. S3). Similar heavy REC8 bands have been observed in yeast and 189 mice and represent phosphorylated forms (Watanabe and Nurse 1999; Kitajima et al. 190 2003). 191

REC8 is the major Arabidopsis kleisin required for meiotic axis polymerization and prevention of non-homologous recombination

195 Localization of cohesin and axis proteins are interdependent in many species (Kim et al. 196 2010: Severson et al. 2009: Storlazzi et al. 2008: Chelvsheva et al. 2005). Therefore. 197 we used immunocytology with epifluorescence and super-resolution structured 198 illumination microscopy (SIM) to analyze Arabidopsis axis proteins ASY1 and ASY3 in 199 rec8 (Fig. 1C-1D). In wild type, ASY1 and ASY3 co-localize along linear axes from 200 leptotene until zygotene (Fig. 1D) (Ferdous et al. 2012). In rec8, ASY1 and ASY3 occur 201 in polycomplexes that persist through mid-prophase I (Fig. 1C-1D). The length of rec8 202 ASY1 polycomplexes was shorter compared to the wild type axis at leptotene 203 (mean=30 μ m vs. 220 μ m, MWW test P=3.02×10⁻¹¹) (Supplemental Table S3). 204 Heterochromatic chromocenters were observed within and apart from ASY1 205 polycomplexes in rec8 (Supplemental Fig. S1C), suggesting they are independent 206 structures. To analyze cohesin and the SC within the centromeres, we immunostained 207 for SMC3 or ZYP1, in combination with fluorescence in situ hybridization (FISH) for the 208 CEN180 satellite repeats (Fig. 1E). At the zygotene-pachytene transition, we observed 209 five CEN180-positive regions through which the SMC3 cohesin and ZYP1 SC signals 210 were continuous and relatively uniform (Fig. 1E). 211

212 To investigate the rec8 chromosome entanglements observed during prophase I, we 213 performed FISH using 45S and 5S rDNA probes (Fig. 1F). This revealed physical 214 connections between non-homologous chromosomes in rec8, not observed in wild type 215 (Fig. 1F). Therefore, abnormal axis polymerization in rec8 is associated with loss of 216 recombination fidelity, leading to non-homologous joint molecules that resolve 217 catastrophically at metaphase I (Fig. 1A and 1F). Although Arabidopsis encodes four α -218 kleisins (REC8/SYN1, SYN2, SYN3 and SYN4), REC8 shows strongest transcription in 219 meiotic RNA-seg data (Supplemental Fig. S4A) (Walker et al. 2018). Furthermore, we 220 measured crossovers in syn2 and syn4 mutants using chiasmata counting and 221 fluorescent tagged lines (FTL), and did not observe significant differences to wild type 222 (Supplemental Fig. S4B–S4D and Supplemental Tables S4–S6).

223 224

225

REC8 is enriched in centromeric heterochromatin

226 To map REC8 localization throughout the genome we performed ChIP-seq using 227 REC8-HA rec8 or REC8-Myc rec8 floral buds (Fig. 2A-2B and Supplemental S5). 228 which contain all stages of meiosis. ChIP and input DNA were sequenced and 229 log₂(ChIP/input) enrichment calculated (Supplemental Table S7). Z-score 230 standardization was applied so that the genome-wide mean equals zero and a value of 231 one equates to one standard deviation from the mean. Biological replicate libraries for 232 REC8-HA ChIP-seq were highly correlated (10 kb r_s =0.99), as were REC8-HA and 233 REC8-Myc (10 kb r_s =0.81), at varying physical scales (Supplemental Fig. S5 and 234 Supplemental Table S8), so REC8-HA data were used for subsequent analyses.

235

236 At the chromosome scale, REC8 enrichment was greatest in the centromeres and in 237 proximal heterochromatin (Fig. 2A-2B). Consequently, we observed positive correlations between REC8 and transposable elements (r_s =0.79), DNA methylation in 238 239 CG ($r_s=0.75$), CHG ($r_s=0.72$) and CHH ($r_s=0.75$) sequence contexts and the 240 heterochromatic histone modifications H3K9me2 (r_s =0.86), H3K27me1 (r_s =0.86) and 241 histone variant H2A.W (r_s =0.90) (Fig. 2A, Supplemental Fig. S6 and Supplemental 242 Table S9) (Stroud et al. 2013; Yelagandula et al. 2014). Nucleosomes, measured via 243 MNase-seq, also show high pericentromeric enrichment and a positive correlation with 244 REC8 (r_s =0.66) (Fig. 2A). In contrast, genome-wide negative correlations between 245 REC8 and gene density (r_s =-0.76), and the gene-associated chromatin modifications 246 H3K4me1 (r_s =-0.70), H3K4me2 (r_s =-0.81), H3K4me3 (r_s =-0.83), H2A.Z (r_s =-0.75) and 247 H3K27me3 (*r*_s=-0.45) were observed (Fig. 2B, Supplemental Fig. S6 and Supplemental 248 Table S9) (Yelagandula et al. 2014). Hence, at the chromosome scale, REC8 249 enrichment is strongly correlated with heterochromatin, although substantial signal 250 occurs in the gene-rich chromosome arms. To validate ChIP specificity we analyzed 251 REC8 peak loci using qPCR in REC8-HA rec8 compared to untagged wild type, and 252 observed significant enrichment in all cases (Fig. 2C and Supplemental Table S10).

253

254 Hi-C studies have revealed A/B compartment organization in plant genomes, where the 255 A compartment contains gene-rich euchromatin and the B compartment contains the 256 centromeres and heterochromatin (Feng et al. 2014; Liu et al. 2016). We compared 257 REC8 ChIP-seq data to a high resolution Hi-C map generated from Arabidopsis 258 seedlings (Fig. 2D) (Liu et al. 2016). Hi-C Eigenvalues correspond to the first principle 259 component of the contact matrix, where the sign of the value denotes the compartment 260 (negative=A, positive=B) (Liu et al. 2016). Hi-C Eigenvalues showed a strong positive 261 correlation with REC8 ($r_s=0.70$) (Fig. 2D), indicating enrichment in the B compartment. 262 We compared REC8 ChIP enrichment with cytogenetic maps made at pachytene that 263 relate meiotic axis length (µm) to physical DNA length (kb) (Fransz et al. 2000). For 264 example, the chromosome 4 heterochromatic knob contains 614 kb/µm, compared to

euchromatic regions with a mean of 356 kb/µm (Supplemental Table S11) (Fransz et al.
2000). Differential condensation of these regions is reflected by a 43-fold difference in
REC8 ChIP-seq enrichment (Supplemental Table S11). Therefore, A/B compartment
structure is likely a dominant feature of both mitotic and meiotic chromosomes in
Arabidopsis, consistent with pronounced heterochromatin differentiation at pachytene
(Fig. 1A–1B) (Fransz et al. 2000).

271 272

REC8 anti-correlates with meiotic DSBs and crossovers

273 274 We investigated the relationships between REC8, meiotic DSBs mapped using 275 SPO11-1-oligos, and 3,320 crossovers mapped by genotyping-by-sequencing of 276 Col×Ler F₂ individuals (Choi et al. 2018; Underwood et al. 2018). At the chromosome 277 scale, SPO11-1-oligos and crossovers show negative correlations with REC8 (r_s =-0.22 278 and $r_s=-0.15$), and these relationships are strengthened in the pericentromeres ($r_s=-$ 279 0.94 and r_s =-0.84) (Fig. 3A and Supplemental Fig. S6). However, variation in the ratio 280 of SPO11-1-oligos, crossovers and REC8 was observed along the chromosomes (Fig. 281 3A). Multiple factors likely contribute to this variation, including patterns of interhomolog 282 polymorphism, chromatin states and the action of crossover interference.

283

We previously observed SPO11-1 immunostaining in association with ASY1 284 285 throughout prophase I (Choi et al. 2018). To provide further insight into SPO11-1 286 binding to the genome we performed ChIP-seq, using the SPO11-1-Myc line previously 287 used for SPO11-1-oligo sequencing (Supplemental Table S9) (Choi et al. 2018). At the 288 chromosome scale, SPO11-1 ChIP signal showed a positive correlation with REC8 289 $(r_s=0.64)$ and nucleosomes $(r_s=0.87)$, and a negative correlation with SPO11-1-oligos 290 $(r_s=-0.69)$ and crossovers $(r_s=-0.50)$ (Fig. 3A). Hence, while SPO11-1-oligos capture 291 the DSB landscape, crosslinking of SPO11-1 to chromatin throughout meiosis reveals 292 an axis-associated signal similar to REC8. These data are consistent with recruitment 293 of chromatin loops to axis-associated SPO11-1 during DSB formation and repair (Blat 294 et al. 2002; Panizza et al. 2011).

295

296 At the fine scale, Arabidopsis shows SPO11-1-oligo enrichment in nucleosome-297 depleted gene promoters and terminators (Fig. 3B) (Choi et al. 2018). In contrast, 298 REC8 and SPO11-1 ChIP-seg show strongest enrichment within gene bodies towards 299 transcriptional termination sites (TTSs), and were positively correlated with one another 300 $(r_s=0.98)$ (Fig. 3B). The REC8 profile within genes also strikingly correlates with 301 transcript abundance and nucleosomes (r_s =0.95 and r_s =0.92) (Fig. 3B). We analyzed 302 introns and exons, orientated in gene 5' to 3' directions, and observed that SPO11-1-303 oligos were relatively depleted from exons and enriched within introns, whereas REC8, 304 SPO11-1 ChIP, transcripts and nucleosomes show the opposite trends (Supplemental 305 Fig. S7). This reveals fine-scale variation in the meiotic axis and recombination 306 machinery in relation to gene organization, transcription and chromatin.

307

308 To further analyze REC8 at the fine scale, we identified 87,738 peaks with a mean 309 width of 475 bp (Fig. 3C, Supplemental Fig. S8A and Supplemental Table S12). 310 Consistent with the trends at the chromosome scale and within genes, REC8 peak 311 enrichment positively correlated with nucleosomes (r_s=0.68) and SPO11-1 ChIP 312 (r_s =0.65), but negatively with SPO11-1-oligos (r_s =-0.72) (Fig. 3C). We applied 313 permutation tests and observed that significantly fewer-than-expected REC8 peaks 314 overlap SPO11-1-oligo hotspots and crossovers, and more-than-expected REC8 peaks 315 overlap nucleosome positions and SPO11-1 ChIP peaks (all P<0.0001) (Supplemental 316 Fig. S9 and Supplemental Table S12). We analyzed crossover intervals and 5 kb 317 flanking regions and observed that REC8, nucleosomes and SPO11-1 ChIP were all depleted, whereas SPO11-1-oligos were enriched (Fig. 3D and Supplemental Fig. S8B). Finally, we investigated DNA sequence composition and observed that REC8 peaks and well-positioned nucleosomes show a strong GC bias, whereas SPO11-1oligo hotspots and crossovers are AT-biased (Fig. 3E–3F). Therefore, REC8 enrichment at both the chromosome and the fine scale is associated with suppression of SPO11-1-oligos and crossovers, and correlates with the presence of heterochromatin and GC-rich DNA sequences.

325

REC8-cohesin and meiotic DSB landscapes are remodeled in *kyp suvh5 suvh6* H3K9me2 mutants

328 329 In plants, non-CG DNA methylation and H3K9me2 maintain each other in a self-330 reinforcing epigenetic loop (Stroud et al. 2014, 2013). For example, the kryptonite/suvh4 suvh5 suvh6 (kss) SET domain triple mutant eliminates both 331 332 H3K9me2 and non-CG DNA methylation (Stroud et al. 2014, 2013). Mutants in the 333 non-CG/H3K9me2 pathway also show increased pericentromeric DSBs and 334 crossovers in Arabidopsis (Underwood et al. 2018). Therefore, we performed REC8-335 HA ChIP-seq in kss mutants to test for interactions between cohesin, chromatin and 336 recombination. At the chromosome scale, the kss mutant shows slight but significant 337 changes in REC8 ChIP enrichment, with decreases in the centromeric heterochromatin 338 (one-tailed MWW test P=0.008), and increases in the chromosome arms (one-tailed 339 MWW test P=0.001) (Supplemental Fig. S10). We performed REC8-HA 340 immunostaining in wild type and kss and observed a slight decrease in signal over the 341 heterochromatin, although this was not significant (Supplemental Tables S13-S14). 342 Furthermore, the level of REC8 loading in kss is sufficient to maintain sister 343 chromosome cohesion and no decrease in pollen viability occurs, compared to wild 344 type (MWW test P=0.29) (Fig. 4A and Supplemental Table S15). Hence, REC8 345 function in maintaining cohesion during meiosis is not H3K9me2-dependent in 346 Arabidopsis. To assess chromatin compaction during meiosis, pachytene cells were 347 DAPI-stained and the proportion of area occupied by heterochromatin measured. A 348 slight but significant decrease in heterochromatic compaction was observed in kss 349 (MWW test P=0.047) (Supplemental Table S16), which is consistent with changes to 350 Hi-C contact maps in kss heterochromatin (Feng et al. 2014).

351

352 We next analyzed REC8, chromatin and recombination in wild type versus kss mutants 353 at the fine scale. For example, 15,562 hypo-CHG differentially DNA methylated regions 354 (DMRs) were previously identified in kss (Stroud et al. 2013), which in wild type are 355 nucleosome-enriched and DSB-suppressed (Fig. 4B). We observed that these hypo-356 CHG DMRs lose both REC8 and H3K9me2, and gain SPO11-1-oligos in kss (onetailed MWW tests, all P<2.2×10⁻¹⁶) (Fig. 4B). As a further test we analyzed H3K9me2 357 peaks defined in wild type (n=20,289), which showed a similar pattern to hypo-CHG 358 359 DMRs, with coincident loss of H3K9me2, non-CG DNA methylation and REC8 and gain of SPO11-1-oligos in kss (all P<2.2×10⁻¹⁶) (Fig. 4C). We used ChIP-qPCR to 360 analyze enrichment at REC8 peaks observed to lose both REC8 and H3K9me2 in kss 361 362 (Fig. 4D and Supplemental Table S17). Using independent ChIP replicates this assay 363 confirmed reduction of REC8 at the peak loci in kss, compared to a control locus that 364 did not change (Fig. 4D and Supplemental Table S17).

365

We previously observed that DNA and RNA transposons are differentiated by chromatin state and levels of meiotic recombination in Arabidopsis (Choi et al. 2018). Compared to DNA elements, RNA elements show higher REC8 and nucleosomes, and lower SPO11-1-oligos (Fig. 4E–4G and Supplemental Fig. S11) (Choi et al. 2018). RNA elements also show higher H3K9me2 and non-CG methylation levels in wild type, which are reduced in *kss* (Fig. 4E–4F). As observed at hypo-CHG DMRs, loss of heterochromatic marks at RNA elements correlates with reduced REC8 and gain of SPO11-1-oligos in *kss* (Fig. 4E–4F). In contrast, DNA elements also show loss of heterochromatic marks in *kss*, while REC8 was unchanged (Fig. 4E–4G). Hence, REC8, recombination and chromatin are differentiated across transposon classes, with greatest cohesin accumulation on heterochromatic RNA elements that are highly enriched in proximity to the centromeres.

378

379 **REC8** enrichment in genes anti-correlates with transcription levels

380 381 Cohesin occupancy on chromosomes is strongly influenced by transcription 382 (Busslinger et al. 2017; Lengronne et al. 2004; Misulovin et al. 2008; Kagey et al. 2010; 383 Sun et al. 2015). Therefore, we compared REC8 enrichment with RNA-seq data 384 generated from wild type meiotic-stage floral buds, or directly from male meiocytes (Fig. 385 5A) (Walker et al. 2018; Choi et al. 2018). In both cases we observed an anti-386 correlation between RNA expression and REC8 enrichment at the chromosome scale 387 $(r_s=-0.80 \text{ and } r_s=-0.66)$ (Fig. 5A). Within gene bodies, REC8 enrichment was spatially 388 correlated with RNA expression ($r_s=0.95$), H3K4me1 ($r_s=0.87$) and CG DNA 389 methylation ($r_s=0.95$), whereas negative correlations were observed between REC8 390 and chromatin modifications enriched at gene 5' ends, including H3K4me3 (r_s =-0.64), 391 H3K4me2 (r_s =-0.49) and H2A.Z (r_s =-0.64) (Fig. 5B). Therefore, REC8 accumulates 392 within gene bodies, spatially coincident with chromatin marks associated with active 393 transcription (H3K4me1 and CG methylation).

394

395 To further investigate the relationship between transcription levels and REC8, we 396 ranked genes into six groups (hexiles), according to REC8 enrichment within 397 transcribed regions (TSSs-TTSs) (Fig. 5C and Supplemental Fig. S12). Average REC8 398 and transcription levels were negatively correlated (r_s =-0.44), with highly transcribed 399 genes showing lowest REC8 (Fig. 5C). Reciprocal patterns were observed when genes 400 were ranked according to transcription, with low-expression genes showing highest 401 REC8 (Supplemental Fig. S13). In addition, polarized REC8 enrichment occurs 402 towards the TTS of gene hexiles with highest transcription (Fig. 5C), consistent with 403 RNA polymerase pushing or evicting cohesin along transcribed genes. Gene hexiles 404 with highest REC8 also show highest nucleosomes and H3K27me3 levels, lowest 405 H3K4me3 and H2A.Z spreading throughout the gene body (Fig. 5C), which are 406 features of facultatively silent genes in plants (Mozgova and Hennig 2015). 407 Interestingly, analysis of H3K27me3 in relation to REC8 peaks showed enrichment in 408 flanking positions, although the peaks themselves were depleted of this mark 409 (Supplemental Fig. S8A). In conclusion, we observe intragenic REC8 enrichment, with 410 highest levels in genes that are transcriptionally silenced by the Polycomb system and 411 H3K27me3.

412

413 We performed RNA-seq from wild type and kss floral buds and compared these data to 414 REC8, SPO11-1-oligo and DNA methylation data (Fig. 5D). Genes in wild type show 415 low levels of CHG DNA methylation, which was further reduced in kss (Fig. 5D). We 416 observed that gene promoters and terminators show increased REC8 and reduced 417 SPO11-1-oligos in kss, whereas opposite trends are observed within gene bodies (Fig. 418 5E). We performed differential expression analysis and identified 179 transposable 419 elements (TEs) and 263 genes that were transcriptionally upregulated in kss 420 (FDR<0.01) (Supplemental Fig. S14 and Supplemental Table S18). We observed 421 reduced REC8 and gain of SPO11-1-oligos over the upregulated genes and TEs. 422 coincident with loss of CHG DNA methylation (Fig. 5E-5F). These loci provide 423 examples of local changes to chromatin state and transcription that influence REC8
424 occupancy and recombination, within both genes and transposons.
425

426 Axis polycomplexes in *rec8* recruit the homologous recombination machinery 427 with altered stoichiometry

428

429 Our genomic data revealed that REC8 accumulates in regions of low meiotic DSBs and 430 crossovers in Arabidopsis. We were therefore interested to further investigate the 431 cause of meiotic chromosome fragmentation in rec8. As we observed evidence for 432 non-homologous recombination in rec8 using FISH (Fig. 1F), we hypothesized that 433 rec8 axis polycomplexes may recruit the recombination machinery. To visualize meiotic 434 DSBs, we immunostained male meiocytes for yH2A.X and observed a mean of 202 435 axis foci in wild type (Fig. 6A and Supplemental Table S19). In rec8, yH2A.X foci were significantly reduced (mean=53, MWW test $P=3.37 \times 10^{-6}$), although they remained 436 437 associated with ASY1 polycomplexes (Fig. 6A and Table S19). We immunostained for 438 the ssDNA binding proteins RPA1a, RAD51 and DMC1, which show mean axis-439 associated foci numbers of 181, 174 and 172 respectively at mid-prophase I in wild 440 type, which were significantly reduced in rec8 to 39, 36 and 14 (MWW tests, 441 P=3.37×10⁻⁶, P=3.33×10⁻⁶, P=1.08×10⁻⁵) (Fig. 6B–6C, Supplemental Fig. S15A and 442 Supplemental Tables S19-S20). We also immunostained for SPO11-1-Myc and 443 observed foci distributed throughout the nucleus that were axis-associated at leptotene 444 and persisted until pachytene (Supplemental Fig. S15B and Supplemental Table S21). 445 In rec8, SPO11-1-Myc signal was distributed throughout the nucleus, both within and 446 apart from ASY1 polycomplexes (Supplemental Fig. S15B). The presence of SPO11-1 447 in regions lacking axis polycomplexes in rec8, which also show an absence of DSB 448 markers, is consistent with the axis being required to promote DSBs (Supplemental Fig. 449 S15B). In support of this, a positive correlation exists between axis length and vH2A.X 450 and RAD51 foci between nuclei, in both wild type and rec8 (wild type $r_s=0.83$ and 0.69, 451 $rec8 r_s=0.92$ and 0.77) (Supplemental Table S22). Together, this provides cytological 452 evidence that DSB formation and interhomolog strand invasion are associated with 453 rec8 axis polycomplexes.

454

455 We next immunostained for ZMM repair factors, which are required for formation of 456 interfering crossovers (Hunter 2015). In wild type, the MutS homolog MSH4 forms a 457 mean of 179 axis-associated foci at leptotene, which were significantly reduced in rec8 (mean=13 foci, MWW test $P=1.10\times10^{-5}$) (Fig. 6D and Supplemental Table S20). The 458 459 MutL homolog MLH1 acts late in prophase I and shows a mean of 10.4 chiasmata-460 associated foci at diakinesis, which were also significantly reduced in rec8, yet remained associated with the entangled chromosomes at late prophase I (mean=4.9 461 foci, MWW test P=2.59×10⁻¹⁰) (Fig. 6E and Supplemental Table S23). It is notable that 462 463 MSH4 and DMC1 foci showed a greater reduction in foci numbers (7.3% and 8.3% of 464 wild type), compared with γH2A.X, RAD51, RPA1a and MLH1 (26.2%, 19.9%, 22.4% 465 and 47% of wild type) (Supplemental Fig. S15C and Supplemental Tables S19–S20 466 and S23). Therefore, although rec8 polycomplexes recruit recombination foci, they are 467 reduced in number and show altered stoichiometry relative to wild type. We propose 468 that a subset of these foci represent non-homologous recombination events in rec8 469 that lead to joint molecules and fragmentation at metaphase I.

470

We used immunocytology with epifluorescence and SIM to analyze Arabidopsis axis (ASY1, ASY3 and SMC3) and SC (ZYP1) components in wild type and *rec8* (Fig. 6F– 6I). Chromosome synapsis initiates at zygotene with the formation of ZYP1 stretches, which become depleted of ASY1 (Fig. 6F), until full synapsis is achieved at pachytene (Ferdous et al. 2012). We observed short stretches of ZYP1 polymerization between 476 ASY1 polycomplexes in rec8 (Fig. 6F). In wild type ZYP1 polymerizes between axes 477 separated by a mean distance of 109 nm (Fig. 6G and Supplemental Table S24). 478 consistent with eukaryotic SC widths (Zickler and Kleckner 1999). In rec8, ZYP1 was 479 detected between ASY1 polycomplexes, with a mean distance not significantly different 480 from wild type (119 nm, MWW test P=0.22) (Fig. 6G and Supplemental Table S24). 481 PCH2 is a conserved meiotic AAA+ATPase required to remodel the axis during 482 synapsis, which forms a linear signal with ZYP1 at pachytene (Fig. 6H) (Lambing et al. 483 2015). The rec8 polycomplexes co-stained for both PCH2 and ZYP1 (Fig. 6H). 484 Interestingly, the SMC3 cohesin subunit was recruited to ASY1 polycomplexes, despite 485 the absence of REC8 (Fig. 6I). Therefore, rec8 polycomplexes include ASY1, ASY3 486 and SMC3 and can recruit PCH2 and ZYP1 to produce synapsed structures with a 487 similar inter-axis width to wild type. These cytological data support a role for REC8-488 cohesin in organizing correct polymerization of the axis and SC and promoting high-489 fidelity interhomolog recombination.

490

491 **Discussion**:

492

493 During meiosis, replicated sister chromatids are organized as linear loop arrays 494 connected to the axis, where REC8 is enriched (Zickler and Kleckner 1999; Blat et al. 495 2002; Panizza et al. 2011). Comparative analysis across eukaryotes supports a 496 conserved density of ~20 chromatin loops per µm of axis at pachytene, with larger 497 genomes having increased axis length and/or chromatin loop size (Zickler and 498 Kleckner 1999). The 125 Mb Arabidopsis genome has an axis length of 331 µm 499 equating to 378 kb/µm (Fransz et al. 2000). Assuming 20 loops per µm, this gives an 500 estimate of 18.9 kb per loop (Fig. 7). Cytogenetic maps have also revealed that 501 heterochromatin is more condensed (614 kb/µm) than euchromatic regions (356 502 kb/µm) at pachytene (Fransz et al. 2000), equating to loop size estimates of 30.7 kb 503 and 17.8 kb, respectively (Fig. 7). However, Arabidopsis meiotic chromosome spreads 504 show that chromatin loops extend ~300 nm from the axis, which does not vary between 505 euchromatin and heterochromatin (Ferdous et al. 2012; Armstrong et al. 2002). 506 Therefore, to accommodate additional sequence per µm of axis, the heterochromatic 507 loops must be more highly condensed (Fig. 7). This may enhance REC8 crosslinking to 508 heterochromatin during ChIP, and is also reflected by interphase chromocenter 509 organization and B-compartment identity (Liu et al. 2016; Feng et al. 2014; Fransz et al. 510 2000). It is also important to note that REC8 is lost from the chromosome arms at \sim 30 511 hours post S-phase, whereas it persists in the centromeres until ~33 hours (Cai et al. 512 2003; Chelysheva et al. 2005). As we sample over all meiotic stages, this may further 513 contribute to relative centromeric REC8 ChIP enrichment. 514

515 We tested the role of non-CG DNA methylation and H3K9me2 in REC8 loading using kss mutants (Stroud et al. 2013, 2014). We observed remodeling of REC8 occupancy 516 517 in kss, with regions that lose H3K9me2 and non-CG DNA methylation showing cohesin 518 depletion and gain of SPO11-1-oligos. This is consistent with cohesin and 519 heterochromatin jointly suppressing meiotic DSBs, and is reflected by the shared 520 preference of REC8 and nucleosomes for GC-rich sequences. In contrast, SPO11-1-521 oligo and crossover hotspots are AT-biased. Unlike in fission yeast clr4 or swi6 522 mutants, which lose heterochromatic H3K9me2 and centromere cohesion (Bernard et 523 al. 2001; Nonaka et al. 2002; Mizuguchi et al. 2014; Ellermeier et al. 2010), 524 Arabidopsis kss mutants retain sufficient centromeric REC8 to maintain sister cohesion. 525 Hence, Arabidopsis more closely resembles mouse suv39h1 suv39h2 H3K9me2 526 mutants, where mitotic cohesin is recruited to heterochromatin, but with remodeling on 527 major versus minor satellite repeats (Koch et al. 2008; Guenatri et al. 2004). We 528 propose that in plant and mammalian genomes additional heterochromatic features act

529 redundantly with H3K9me2 to recruit and maintain cohesin in the centromeres. 530 Interestingly, we observed SPO11-1 ChIP enrichment in the centromeres, coincident 531 with elevated REC8 and nucleosome density. Hence, although SPO11-1 is axis-532 enriched in proximity to the heterochromatic loops, these sequences are not efficiently 533 recruited to form DSBs or crossovers during meiosis (Fig. 7).

534

535 Transcription drives cohesin occupancy in diverse eukaryotes (Lengronne et al. 2004; 536 Bausch et al. 2007; Sun et al. 2015; Busslinger et al. 2017). Consistently, we observed 537 a negative relationship between transcription level and REC8-cohesin occupancy 538 within Arabidopsis genes. Hi-C contact maps in fission and budding yeast, which like 539 plants lack CTCF, display contact associations at gene scale termed 'globules' and 540 'crinkles' that relate to transcription (Hsieh et al. 2015; Mizuguchi et al. 2014). High-541 resolution Hi-C studies in Arabidopsis have revealed contact associations over single 542 genes, where 5' and 3' ends interact (Liu et al. 2016). The role of cohesin in intragenic 543 contacts is unknown, although this may relate to the REC8 enrichment we observed 544 within gene bodies. We identified transcriptionally upregulated genes and transposons 545 in kss, which showed depletion of REC8 and gain of SPO11-1-oligos. This is consistent 546 with an important role for transcription in shaping cohesin occupancy in plants. It is also 547 important to consider that plant heterochromatin is actively transcribed by Pol IV and 548 Pol V RNA polymerases, which produce short transcripts required for RNA-directed 549 DNA methylation (Law and Jacobsen 2010). Hence, it will be interesting to explore the 550 effects of heterochromatic transcription on cohesin occupancy in plant centromeric 551 regions.

552

553 Recombination suppression in proximity to the centromeres by cohesin and 554 heterochromatin is important for fertility, as crossovers within these regions can cause 555 aneuploidy (Lamb et al. 2005; Rockmill et al. 2006). Plant centromeres are flanked by 556 large domains of transposon-dense pericentromeric heterochromatin (Law and 557 Jacobsen 2010). As a consequence, plant chromosomes show pronounced telomere-558 centromere gradients of recombination, epigenetic modifications, cohesin enrichment, 559 compartment identity and gene/transposon composition (Higgins et al. 2012; Feng et al. 560 2014; Choi et al. 2018). These gradients likely exert a profound effect on sequence 561 diversity along the length of plant chromosomes and contribute to their functional 562 stratification and evolution. Indeed, genetic variation in REC8 and meiotic axis genes 563 has been identified as targets of selection during polyploid evolution in Arabidopsis 564 arenosa (Yant et al. 2013; Wright et al. 2015). This effect is likely via modification of 565 crossover patterns and stabilization of polyploid chromosome inheritance (Yant et al. 566 2013: Wright et al. 2015). Hence, far from being static components of plant genome 567 architecture, REC8-cohesin and the meiotic axis dynamically evolve and influence 568 patterns of recombination and diversity. 569

570 Acknowledgements:

571

572 We thank Mathilde Grelon for the MLH1 antibody, Paul Fransz for discussions 573 concerning cytological data, Chang Liu for providing Hi-C data and the Gurdon Institute 574 for access to microscopes. Research was supported by grants from the ERC 575 (SynthHotSpot) and BBSRC (BB/L006847/1 and BB/N007557/1), an EMBO long term 576 postdoctoral fellowship (ALTF 807-2009) and a Gatsby Foundation Sainsbury 577 studentship GAT3401. The authors declare no competing interests.

- 578
- 579
- 580
- 581

582 Author Contributions:

583

584 Conceptualization: CL, AJT, KC, JH, FCHF, IRH. Software: AJT, XZ, IRH. 585 Investigation: CL, KC, SDT, PCK, ARB, JH. Writing: CL, AJT, KC, ARB, KO, JH, FCHF, 586 IRH. 587

588 References:589

- Acquaviva L, Székvölgyi L, Dichtl B, Dichtl BS, de La Roche Saint André C, Nicolas A,
 Géli V. 2013. The COMPASS subunit Spp1 links histone methylation to initiation
 of meiotic recombination. *Science* 339: 215–8.
- Armstrong SJ, Caryl AP, Jones GH, Franklin FCH. 2002. Asy1, a protein required for
 meiotic chromosome synapsis, localizes to axis-associated chromatin in
 Arabidopsis and Brassica. *J Cell Sci* 115: 3645–55.
- Baudat F, Imai Y, de Massy B. 2013. Meiotic recombination in mammals: localization
 and regulation. *Nat Rev Genet* 14: 794–806.
- Bausch C, Noone S, Henry JM, Gaudenz K, Sanderson B, Seidel C, Gerton JL. 2007.
 Transcription alters chromosomal locations of cohesin in Saccharomyces
 cerevisiae. *Mol Cell Biol* 27: 8522–32.
- Bernard P, Maure JF, Partridge JF, Genier S, Javerzat JP, Allshire RC. 2001.
 Requirement of Heterochromatin for Cohesion at Centromeres. *Science (80-)*294: 2539–2542.
- Blat Y, Protacio RU, Hunter N, Kleckner N. 2002. Physical and functional interactions
 among basic chromosome organizational features govern early steps of meiotic
 chiasma formation. *Cell* **111**: 791–802.
- 607 Borde V, Robine N, Lin W, Bonfils S, Géli V, Nicolas A. 2009. Histone H3 lysine 4 608 trimethylation marks meiotic recombination initiation sites. *EMBO J* **28**: 99–111.
- Busslinger GA, Stocsits RR, van der Lelij P, Axelsson E, Tedeschi A, Galjart N, Peters
 J-M. 2017. Cohesin is positioned in mammalian genomes by transcription, CTCF
 and Wapl. *Nature* 544: 503–507.
- 612 Cai X, Dong F, Edelmann RE, Makaroff CA. 2003. The Arabidopsis SYN1 cohesin
 613 protein is required for sister chromatid arm cohesion and homologous
 614 chromosome pairing. *J Cell Sci* **116**: 2999–3007.
- Chelysheva L, Diallo S, Vezon D, Gendrot G, Vrielynck N, Belcram K, Rocques N,
 Márquez-Lema A, Bhatt AM, Horlow C, et al. 2005. AtREC8 and AtSCC3 are
 essential to the monopolar orientation of the kinetochores during meiosis. *J Cell Sci* 118: 4621–32.
- Choi K, Zhao X, Kelly KA, Venn O, Higgins JD, Yelina NE, Hardcastle TJ, Ziolkowski
 PA, Copenhaver GP, Franklin FCH, et al. 2013. Arabidopsis meiotic crossover hot
 spots overlap with H2A.Z nucleosomes at gene promoters. *Nat Genet* 45: 1327–
 36.
- Choi K, Zhao X, Tock AJ, Lambing C, Underwood CJ, Hardcastle TJ, Serra H, Kim J,
 Cho HS, Kim J, et al. 2018. Nucleosomes and DNA methylation shape meiotic
 DSB frequency in Arabidopsis thaliana transposons and gene regulatory regions. *Genome Res* doi: 10.1101/gr.225599.117.
- Ellermeier C, Higuchi EC, Phadnis N, Holm L, Geelhood JL, Thon G, Smith GR. 2010.
 RNAi and heterochromatin repress centromeric meiotic recombination. *Proc Natl Acad Sci U S A* 107: 8701–5.
- Feng S, Cokus SJ, Schubert V, Zhai J, Pellegrini M, Jacobsen SE. 2014. Genomewide Hi-C analyses in wild-type and mutants reveal high-resolution chromatin
 interactions in Arabidopsis. *Mol Cell* 55: 694–707.
- Ferdous M, Higgins JD, Osman K, Lambing C, Roitinger E, Mechtler K, Armstrong SJ,
 Perry R, Pradillo M, Cuñado N, et al. 2012. Inter-homolog crossing-over and

synapsis in Arabidopsis meiosis are dependent on the chromosome axis protein
AtASY3. *PLoS Genet* 8: e1002507.

- Fransz PF, Armstrong S, de Jong JH, Parnell LD, van Drunen C, Dean C, Zabel P,
 Bisseling T, Jones GH. 2000. Integrated cytogenetic map of chromosome arm 4S
 of A. thaliana: structural organization of heterochromatic knob and centromere
 region. *Cell* **100**: 367–76.
- 641 Gligoris T, Löwe J. 2016. Structural Insights into Ring Formation of Cohesin and 642 Related Smc Complexes. *Trends Cell Biol* **26**: 680–693.
- Guenatri M, Bailly D, Maison C, Almouzni G. 2004. Mouse centric and pericentric
 satellite repeats form distinct functional heterochromatin. *J Cell Biol* 166: 493–505.
- Higgins JD, Perry RM, Barakate A, Ramsay L, Waugh R, Halpin C, Armstrong SJ,
 Franklin FCH. 2012. Spatiotemporal asymmetry of the meiotic program underlies
 the predominantly distal distribution of meiotic crossovers in barley. *Plant Cell* 24:
 4096–109.
- Higgins JD, Sanchez-Moran E, Armstrong SJ, Jones GH, Franklin FCH. 2005. The
 Arabidopsis synaptonemal complex protein ZYP1 is required for chromosome
 synapsis and normal fidelity of crossing over. *Genes Dev* 19: 2488–2500.
- Hsieh T-HS, Weiner A, Lajoie B, Dekker J, Friedman N, Rando OJ. 2015. Mapping
 Nucleosome Resolution Chromosome Folding in Yeast by Micro-C. *Cell* 162: 108–
 19.
- Hunter N. 2015. Meiotic Recombination: The Essence of Heredity. *Cold Spring Harb Perspect Biol* **7**: a016618.
- Imai Y, Baudat F, Taillepierre M, Stanzione M, Toth A, de Massy B. 2017. The PRDM9
 KRAB domain is required for meiosis and involved in protein interactions. *Chromosoma* 681–695.
- Janssen A, Colmenares SU, Karpen GH. 2018. Heterochromatin: Guardian of the
 Genome. Annu Rev Cell Dev Biol 34: 265–288.
- Kagey MH, Newman JJ, Bilodeau S, Zhan Y, Orlando DA, van Berkum NL, Ebmeier
 CC, Goossens J, Rahl PB, Levine SS, et al. 2010. Mediator and cohesin connect
 gene expression and chromatin architecture. *Nature* 467: 430–435.
- Keeney S, Giroux CN, Kleckner N. 1997. Meiosis-specific DNA double-strand breaks
 are catalyzed by Spo11, a member of a widely conserved protein family. *Cell* 88:
 375–84.
- Kim KP, Weiner BM, Zhang L, Jordan A, Dekker J, Kleckner N. 2010. Sister cohesion
 and structural axis components mediate homolog bias of meiotic recombination.
 Cell 143: 924–37.
- Kitajima TS, Miyazaki Y, Yamamoto M, Watanabe Y. 2003. Rec8 cleavage by
 separase is required for meiotic nuclear divisions in fission yeast. *EMBO J* 22:
 5643–53.
- Klein F, Mahr P, Galova M, Buonomo SB, Michaelis C, Nairz K, Nasmyth K. 1999. A
 central role for cohesins in sister chromatid cohesion, formation of axial elements,
 and recombination during yeast meiosis. *Cell* **98**: 91–103.
- Koch B, Kueng S, Ruckenbauer C, Wendt KS, Peters J-M. 2008. The Suv39h–HP1
 histone methylation pathway is dispensable for enrichment and protection of
 cohesin at centromeres in mammalian cells. *Chromosoma* **117**: 199–210.
- Lamb NE, Sherman SL, Hassold TJ. 2005. Effect of meiotic recombination on the
 production of aneuploid gametes in humans. *Cytogenet Genome Res* 111: 250–5.
- Lambing C, Osman K, Nuntasoontorn K, West A, Higgins JD, Copenhaver GP, Yang J,
 Armstrong SJ, Mechtler K, Roitinger E, et al. 2015. Arabidopsis PCH2 Mediates
 Meiotic Chromosome Remodeling and Maturation of Crossovers. *PLoS Genet* 11:
 e1005372.
- Law JA, Jacobsen SE. 2010. Establishing, maintaining and modifying DNA methylation
 patterns in plants and animals. *Nat Rev Genet* **11**: 204–220.

- Lengronne A, Katou Y, Mori S, Yokobayashi S, Kelly GP, Itoh T, Watanabe Y,
 Shirahige K, Uhlmann F. 2004. Cohesin relocation from sites of chromosomal
 loading to places of convergent transcription. *Nature* 430: 573–578.
- Liu C, Wang C, Wang G, Becker C, Zaidem M, Weigel D. 2016. Genome-wide analysis
 of chromatin packing in *Arabidopsis thaliana* at single-gene resolution. *Genome Res* 26: 1057–1068.
- Maloisel L, Rossignol JL. 1998. Suppression of crossing-over by DNA methylation in
 Ascobolus. *Genes Dev* 12: 1381–9.
- Misulovin Z, Schwartz YB, Li X-Y, Kahn TG, Gause M, MacArthur S, Fay JC, Eisen MB,
 Pirrotta V, Biggin MD, et al. 2008. Association of cohesin and Nipped-B with
 transcriptionally active regions of the Drosophila melanogaster genome. *Chromosoma* 117: 89–102.
- Mizuguchi T, Fudenberg G, Mehta S, Belton J-M, Taneja N, Folco HD, FitzGerald P,
 Dekker J, Mirny L, Barrowman J, et al. 2014. Cohesin-dependent globules and
 heterochromatin shape 3D genome architecture in S. pombe. *Nature* 516: 432–
 435.
- Mozgova I, Hennig L. 2015. The Polycomb Group Protein Regulatory Network. *Annu Rev Plant Biol* 66: 269–296.
- Nambiar M, Smith GR. 2018. Pericentromere-Specific Cohesin Complex Prevents
 Meiotic Pericentric DNA Double-Strand Breaks and Lethal Crossovers. *Mol Cell*.
- Nasmyth K, Haering CH. 2009. Cohesin: Its Roles and Mechanisms. *Annu Rev Genet*43: 525–558.
- Nonaka N, Kitajima T, Yokobayashi S, Xiao G, Yamamoto M, Grewal SIS, Watanabe Y.
 2002. Recruitment of cohesin to heterochromatic regions by Swi6/HP1 in fission
 yeast. *Nat Cell Biol* 4: 89–93.
- Pan J, Sasaki M, Kniewel R, Murakami H, Blitzblau HG, Tischfield SE, Zhu X, Neale
 MJ, Jasin M, Socci ND, et al. 2011. A hierarchical combination of factors shapes
 the genome-wide topography of yeast meiotic recombination initiation. *Cell* 144:
 716 719–31.
- Panizza S, Mendoza MA, Berlinger M, Huang L, Nicolas A, Shirahige K, Klein F. 2011.
 Spo11-accessory proteins link double-strand break sites to the chromosome axis
 in early meiotic recombination. *Cell* 146: 372–83.
- Parvanov ED, Tian H, Billings T, Saxl RL, Spruce C, Aithal R, Krejci L, Paigen K,
 Petkov PM. 2017. PRDM9 interactions with other proteins provide a link between
 recombination hotspots and the chromosomal axis in meiosis ed. Y.M. Yamashita. *Mol Biol Cell* 28: 488–499.
- Peters J-M, Tedeschi A, Schmitz J. 2008. The cohesin complex and its roles in
 chromosome biology. *Genes Dev* 22: 3089–3114.
- Rockmill B, Voelkel-Meiman K, Roeder GS. 2006. Centromere-proximal crossovers are
 associated with precocious separation of sister chromatids during meiosis in
 Saccharomyces cerevisiae. *Genetics* 174: 1745–1754.
- Severson AF, Ling L, Van Zuylen V, Meyer BJ. 2009. The axial element protein HTP-3
 promotes cohesin loading and meiotic axis assembly in C. elegans to implement
 the meiotic program of chromosome segregation. *Genes Dev* 23: 1763–1778.
- Sommermeyer V, Béneut C, Chaplais E, Serrentino ME, Borde V. 2013. Spp1, a
 member of the Set1 Complex, promotes meiotic DSB formation in promoters by
 tethering histone H3K4 methylation sites to chromosome axes. *Mol Cell* 49: 43–54.
- Stanzione M, Baumann M, Papanikos F, Dereli I, Lange J, Ramlal A, Tränkner D,
 Shibuya H, de Massy B, Watanabe Y, et al. 2016. Meiotic DNA break formation
 requires the unsynapsed chromosome axis-binding protein IHO1 (CCDC36)
 in mice. Nat Cell Biol 18: 1208–1220.
- Storlazzi A, Tesse S, Ruprich-Robert G, Gargano S, Poggeler S, Kleckner N, Zickler D.
 2008. Coupling meiotic chromosome axis integrity to recombination. *Genes Dev*

- **22**: 796–809.
- Stroud H, Do T, Du J, Zhong X, Feng S, Johnson L, Patel DJ, Jacobsen SE. 2014.
 Non-CG methylation patterns shape the epigenetic landscape in Arabidopsis. *Nat Struct Mol Biol* 21: 64–72.
- Stroud H, Greenberg MVC, Feng S, Bernatavichute Y V, Jacobsen SE. 2013.
 Comprehensive analysis of silencing mutants reveals complex regulation of the
 Arabidopsis methylome. *Cell* **152**: 352–64.
- Sun X, Huang L, Markowitz TE, Blitzblau HG, Chen D, Klein F, Hochwagen A. 2015.
 Transcription dynamically patterns the meiotic chromosome-axis interface. *Elife* 4.
- Tanaka T, Cosma MP, Wirth K, Nasmyth K. 1999. Identification of cohesin association
 sites at centromeres and along chromosome arms. *Cell* **98**: 847–58.
- Uhlmann F. 2016. SMC complexes: from DNA to chromosomes. *Nat Rev Mol Cell Biol*17: 399–412.
- Underwood CJ, Choi K, Lambing C, Zhao X, Serra H, Borges F, Simorowski J, Ernst E,
 Jacob Y, Henderson IR, et al. 2018. Epigenetic activation of meiotic recombination
 near Arabidopsis thaliana centromeres via loss of H3K9me2 and non-CG DNA
 methylation. *Genome Res* doi: 10.1101/gr.227116.117.
- Walker J, Gao H, Zhang J, Aldridge B, Vickers M, Higgins JD, Feng X. 2018. Sexuallineage-specific DNA methylation regulates meiosis in Arabidopsis. *Nat Genet* 50:
 130–137.
- Watanabe Y, Nurse P. 1999. Cohesin Rec8 is required for reductional chromosome
 segregation at meiosis. *Nature* 400: 461–4.
- Wright KM, Arnold B, Xue K, ?urinov? M, O?Connell J, Bomblies K. 2015. Selection on
 Meiosis Genes in Diploid and Tetraploid Arabidopsis arenosa. *Mol Biol Evol* 32:
 944–955.
- Yant L, Hollister JDD, Wright KMM, Arnold BJJ, Higgins JDD, Franklin FCHCH,
 Bomblies K. 2013. Meiotic adaptation to genome duplication in Arabidopsis
 arenosa. *Curr Biol* 23: 2151–6.
- Yelagandula R, Stroud H, Holec S, Zhou K, Feng S, Zhong X, Muthurajan UM, Nie X,
 Kawashima T, Groth M, et al. 2014. The histone variant H2A.W defines
 heterochromatin and promotes chromatin condensation in Arabidopsis. *Cell* 158:
 98–109.
- Yelina NE, Lambing C, Hardcastle TJ, Zhao X, Santos B, Henderson IR. 2015. DNA
 methylation epigenetically silences crossover hot spots and controls chromosomal
 domains of meiotic recombination in Arabidopsis. *Genes Dev* 29: 2183–202.
- Zamudio N, Barau J, Teissandier A, Walter M, Borsos M, Servant N, Bourc'his D. 2015.
 DNA methylation restrains transposons from adopting a chromatin signature permissive for meiotic recombination. *Genes Dev* 29: 1256–70.
- Zickler D, Kleckner N. 1999. Meiotic chromosomes: integrating structure and function.
 Annu Rev Genet 33: 603–754.
- 781 782
- 783
- 784
- 785 786
- 787
- 788
- 789
- 790
- 791
- 792
- 793

794 **Figure Legends**:

795

796 Figure 1. Complementation of rec8 meiotic catastrophe via epitope tagging. (A) 797 DAPI-stained spreads of wild type (Col), rec8 and REC8-HA rec8 male meiocytes at 798 the labeled stages of meiosis. (B) Male meiocytes were stained for REC8-HA (red) and 799 DAPI (blue), in the labeled genotypes and stages. (C) SIM images of wild type and 800 rec8 male meiocytes at early prophase I stained for ASY1 (green) and DAPI (blue). (D) 801 As for C, but stained for ASY1 (green), ASY3 (red) and DAPI (blue). Close-ups of rec8 802 axis polycomplexes are shown (lower). White arrows indicate regions staining for ASY1 803 but not ASY3. (E) Male meiocytes at pachytene stained for SMC3 (red) or ZYP1 (red), 804 DAPI (blue) and CEN180 FISH (green). Inset images show zooms of the CEN180-805 positive regions. (F) Male melocytes at metaphase I with FISH performed against 45S 806 (green) and 5S (red) rDNA. The positions of chromosomes 2, 4 and 5 are indicated. All 807 scale bars=10 µm.

808

809 2. Figure Genomic landscapes of **REC8-cohesin**, euchromatin and 810 heterochromatin. (A) Genome-wide profiles (log₂(ChIP/input) of REC8-HA (red) 811 compared with transposable element density, DNA methylation (%) (Stroud et al. 2013), 812 H2A.W (Yelagandula et al. 2014), H3K9me2, H3K27me1 and nucleosomes (blue) 813 (Choi et al. 2018). Vertical solid lines indicate telomeres and dotted lines indicate 814 centromeres. Spearman's correlation coefficients (r_s) are printed above the plots. (B) 815 As for A, but plotting gene density, H3K4me1, H3K4me2, H3K4me3 (Choi et al. 2018), H2A.Z (Yelagandula et al. 2014) and H3K27me3 (blue). (C) ChIP-qPCR enrichment (% 816 817 input) in REC8-HA rec8 and untagged wild type (Col) floral buds at REC8 peaks. (D) 818 REC8-HA ChIP-seq data (black) plotted against Hi-C Eigenvalues (red) that 819 correspond to the first principle component of the contact matrix, where the sign of the 820 value denotes compartment (Liu et al. 2016).

821

822 Figure 3. REC8 enrichment correlates with suppression of meiotic DSBs and 823 crossovers. (A) Genome-wide profiles (log₂(ChIP/input) of REC8-HA (red) compared 824 with SPO11-1-oligos (Choi et al. 2018), SPO11-1 ChIP and crossovers (blue) (Choi et 825 al. 2018). Vertical solid lines indicate telomeres and dotted lines indicate centromeres. 826 Spearman's correlation coefficients (r_s) are printed above. (B) REC8-HA (red), SPO11-827 1-oligos, SPO11-1 ChIP-seq, RNA-seq and nucleosomes (blue) plotted between gene 828 transcriptional start and termination sites (TSS-TTS) and 2 kb flanking regions, 829 compared to the same number of random regions of the same widths. (C) Average 830 coverage profiles of REC8-HA (red) compared with SPO11-1-oligos, SPO11-1 ChIP 831 and nucleosomes (blue) within REC8-HA peaks, compared to the same number of 832 random positions of the same widths. (D) As for C, but plotting over crossover intervals 833 and 5 kb flanking regions, compared to the same number of random positions. Mean 834 resolved crossover widths are shown by dotted lines. (E) Base frequencies (A+T=blue; 835 G+C=red) plotted in 2 kb regions around the midpoints of REC8 peaks or nucleosomes 836 and compared to random positions. (F) As for E, but analyzing SPO11-1-oligo hotspots 837 with 2 kb of flanking sequence, or crossovers with 5 kb.

838

839 Figure 4. REC8, chromatin and meiotic DSB landscapes are remodeled in kyp 840 suvh5 suvh6. (A) DAPI-stained or HA immunostained (red) spreads of wild type and 841 kss male meiocytes at the labeled stages. White arrows indicate chromocenters. All 842 scale bars=10µm. (B) REC8-HA (log₂(ChIP/input)), SPO11-1-oligos, CHG methylation 843 and H3K9me2 from wild type (blue) and kss (red) within hypo-CHG DMRs (Stroud et al. 844 2013), and 2 kb flanking regions, or the same number of random positions of the same 845 widths. The lower plot shows nucleosomes and SPO11-1 ChIP-seq in wild type within 846 the hypo-CHG DMRs. (C) As for B, but plotting in relation to H3K9me2 peaks identified

847 in wild type. (D) Fold change of REC8 ChIP-gPCR enrichment at REC8 peaks in 848 REC8-HA rec8 compared to kss. normalized by Peak 3 which has low H3K9me2 and 849 did not change in kss. Peak 7 is a negative control region not expected to change in 850 kss. (E) As for B, but plotting in relation to DNA transposons. (F) As for B, but plotting 851 in relation to RNA transposons. (G) Bar graphs showing permutation test derived 852 log₂(observed:expected) overlap of REC8 and SPO11-1-oligo peaks in wild type and 853 kss with different transposon families. Vertical gray lines mark significance thresholds 854 (α=0.05).

855

856 Figure 5. REC8 is shaped by chromatin state and transcription within genes and 857 transposons. (A) REC8-HA (log₂(ChIP/input) red) compared with RNA-seq from 858 meiocytes and floral buds (blue) (Walker et al. 2018; Choi et al. 2018). Vertical solid 859 lines indicate telomeres and dotted lines indicate centromeres. Spearman's correlation 860 coefficients (r_s) are printed above the plots. (B) REC8-HA (red) was compared with 861 RNA-seq (Choi et al. 2018), H3K4me1, H3K4me2, H3K4me3, H2A.Z and DNA 862 methylation in CG, CHG and CHH sequence contexts (blue) (Stroud et al. 2013) in 863 gene TSS-TTS and 2 kb flanking regions, or the same number of random regions of 864 the same widths. Spearman's correlation coefficients (r_s) are printed above. (C) As for 865 B, but analyzing the indicated parameters within genes that were ranked into hexiles 866 according to REC8 levels between TSS and TTS (red=highest, blue=lowest). (D) As for 867 B, but analyzing REC8-HA, SPO11-1-oligos or CHG DNA methylation between gene 868 TSS and TTS, or the same number of random positions of the same widths, in wild 869 type (blue) versus kss (red). (E) As for D, but analyzing genes that are transcriptionally 870 upregulated in kss and plotting REC8-HA, SPO11-1-oligos and CHG DNA methylation. 871 (F) As for E, but analyzing transposable elements (TEs) that are transcriptionally 872 upregulated in kss.

873

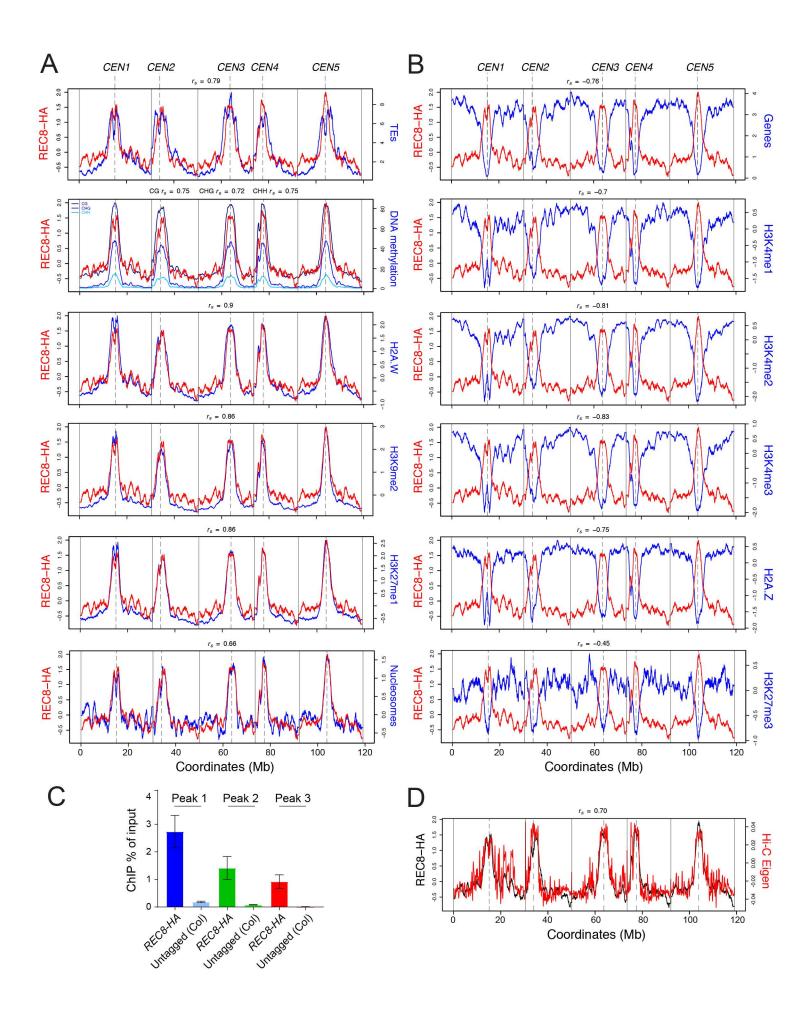
874 Figure 6. Axis polycomplexes recruit the homologous recombination machinery 875 with altered stoichiometry in rec8. (A) Wild type and rec8 male meiocytes in mid-876 prophase I were stained for ASY1 (green), γH2A.X (red) and DAPI (blue). In parts A–D, 877 wild type nuclei are at leptotene. (B) As for A, but staining for RAD51 (red) and ASY1 878 (green). (C) As for A, but staining for DMC1 (red) and ASY1 (green). (D) As for A, but 879 staining for MSH4 (red) and ASY1 (green). (E) As for A, but at diakinesis stage and 880 stained for MLH1 (red) and DAPI (blue). (F) SIM images of male meiocytes at zygotene 881 stage stained for ASY1 (red), ZYP1 (green) and DAPI (blue). Close-ups of synapsed 882 regions are shown in the lower panels, for each genotype. (G) As for F, but showing 883 close-ups of ASY1 (red) and ZYP1 (green) staining. Scale bars=200 nm. (H) As for F, 884 but staining for PCH2 (red), ZYP1 (green) and DAPI (blue). (I) Male meiocytes in mid-885 prophase I stained for ASY1 (green), SMC3 (red) and DAPI (blue). All scale bars=10 886 µm, apart from in (G).

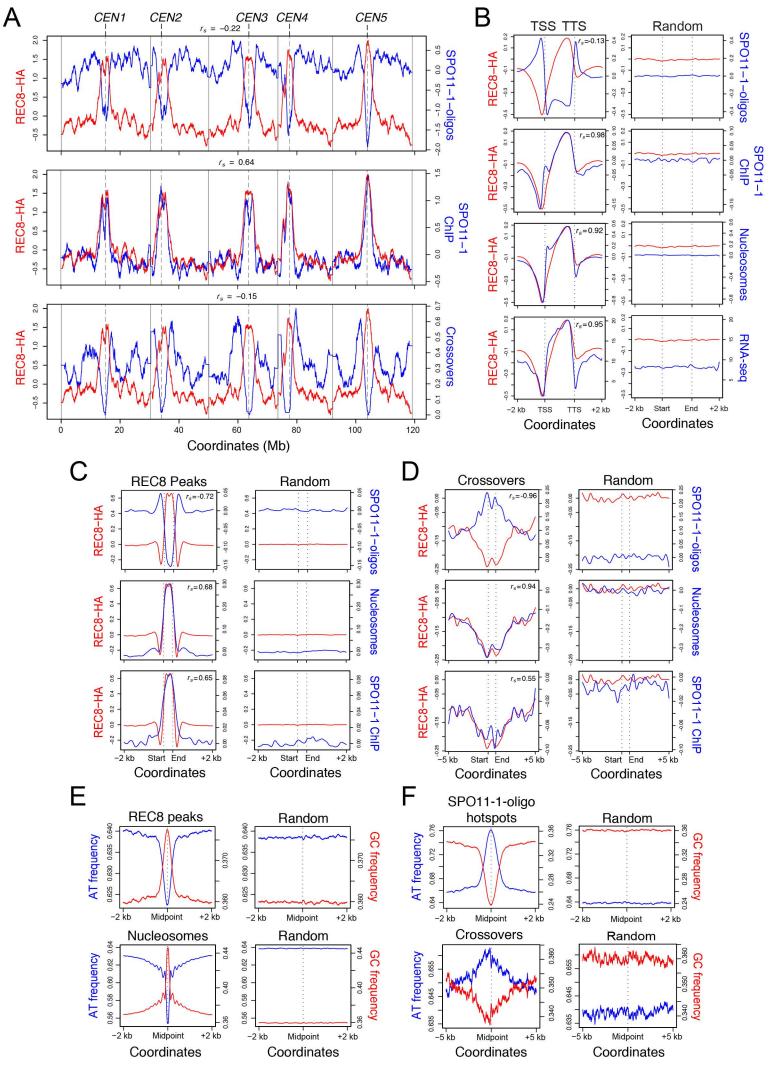
887

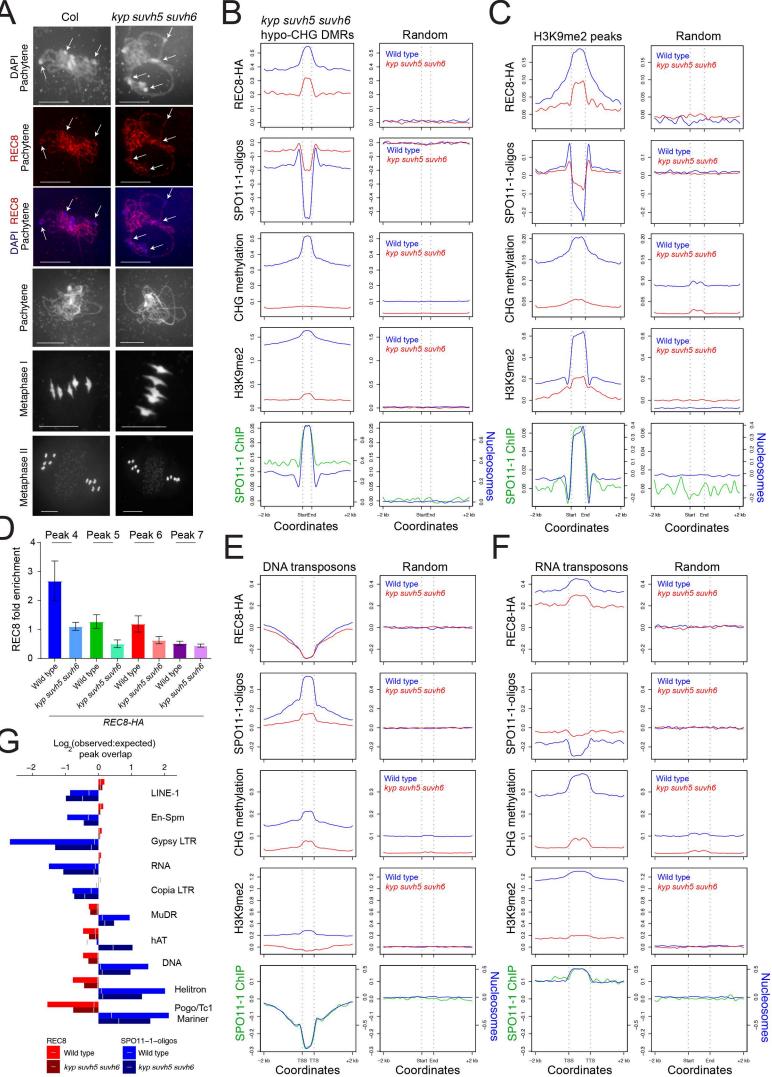
888 Figure 7. Cohesin and chromatin orchestrate meiotic chromosome architecture 889 and interhomolog recombination. (A) Linear loop arrays of sister chromatids (black 890 and blue) are tethered to the meiotic axis at pachytene stage, via passage through 891 REC8-cohesin rings (red). Associated with cohesin are SPO11-1 (green) and the 892 synaptonemal complex protein ZYP1 (purple). Chromatin loops extend from the axis 893 for ~300 nm (Ferdous et al. 2012; Armstrong et al. 2002). A 1 µm section of axis is 894 shown with 20 loops (Zickler and Kleckner 1999), with the physical length of DNA 895 associated with 1 µm of axis inferred from FISH experiments (Fransz et al. 2000). (B) A 896 close-up of A is shown, with one loop beneath corresponding to 600 nm and ~15 kb in 897 euchromatin and ~30 kb in heterochromatin. Chromatin fiber compaction is shown by 898 the black line with nucleosomes (black circles) represented, along with average 899 sequence composition of genes (green), DNA transposons (purple) and RNA transposons (blue). The relative positions of DSBs (red stars) in wild type euchromatin
 and heterochromatin, and in *kyp suvh5 suvh6* heterochromatin, are indicated.

А	DAPI Mid-prophase I	DAPI Metaphase I	DAPI Tetrad	В	DAPI	REC8-HA	DAPI REC8-HA
Wild type (Col)	C)	1 May		REC8-HA rec8 Leptotene			
rec8	-	The.		<i>REC8-HA rec8</i> Pachytene	20		AP.
REC8-HA rec8	DAPI	ASY1	DAPI ASY1	REC8-HA			
Col Mid- prophase I	Calls			Diplotene REC8-HA		* 1	
<i>rec8</i> Mid- prophase I	Ø		trad	<i>rec8</i> Diakinesis		8.	*
D _{Col}	DAPI ASY1	DAPI ASY3	ASY1 ASY3	<i>REC8-HA</i> <i>rec8</i> Metaphase I	·***	·**/*	·**/*
Mid- prophase I <i>rec8</i>				REC8-HA rec8 Somatic			
Mid- prophase I		June 1		Col			
<i>r</i> ec8 Mid- prophase I	()+	Yin	()E	Pachytene			
E	SMC3 CEN180		1 CEN180 DAF	F ۱	DAPI 4	5S <mark>5S</mark> Met	aphase I
Col Pachytene					Col 5 2 4	² 4 5	₄ ^₅ ₄ <i>rec8</i>
Col Pachytene					rec8 2	5 4 2 5 4 2	2 5 4 rec8

bioRxiv preprint doi: https://doi.org/10.1101/512400; this version posted January 4, 2019. The copyright holder for this preprint (which was not certified by peer review) is the author/funder. All rights reserved. No reuse allowed without permission.







Coordinates

Coordinates

Coordinates

